

## RESEARCH ARTICLE

10.1029/2020JD033401

## Atmospheric Processing of Nitrophenols and Nitrocresols From Biomass Burning Emissions

## Key Points:

- Nitrophenols and nitrocresols were primarily produced from NO<sub>3</sub>-initiated oxidation of phenol and cresols, respectively, that originates from either direct biomass burning emissions or the photochemistry of parent aromatic hydrocarbons
- Synergic (photo)oxidative chemistry and physical processes such as dilution and entrainment act as major removal pathways of nitrophenols and nitrocresols
- An appreciable amount of nitrophenols is present in the aerosol water under the humid subtropical weather prevailing in Eastern China; the structural isomerism affects the multiphase partitioning of nitrophenols and nitrocresols

## Supporting Information:

- Supporting Information S1

## Correspondence to:

H. Wang and X. Zhang,  
wanghl@saes.sh.cn;  
xzhang87@ucmerced.edu

## Citation:

Wang, H., Gao, Y., Wang, S., Wu, X., Liu, Y., Li, X., et al. (2020). Atmospheric processing of nitrophenols and nitrocresols from biomass burning emissions. *Journal of Geophysical Research: Atmospheres*, 125, e2020JD033401. <https://doi.org/10.1029/2020JD033401>

Received 28 JUN 2020

Accepted 23 OCT 2020

Accepted article online 3 NOV 2020

## Author Contributions:

**Conceptualization:** Hongli Wang, Yaqin Gao, Ying Liu, Xin Li, Shengrong Lou, Song Guo

**Formal analysis:** Hongli Wang, Yaqin Gao, Siyuan Wang, Xiaokang Wu, Dandan Huang, Geoffrey S. Tyndall, John J. Orlando, Xuan Zhang

**Methodology:** Siyuan Wang, Xiaokang Wu

**Resources:** Shengao Jing, Yingjie Li, Cheng Huang  
(continued)

Hongli Wang<sup>1</sup> , Yaqin Gao<sup>1</sup>, Siyuan Wang<sup>2</sup> , Xiaokang Wu<sup>3</sup> , Ying Liu<sup>4</sup>, Xin Li<sup>4</sup>, Dandan Huang<sup>1</sup>, Shengrong Lou<sup>1</sup> , Zhijun Wu<sup>4</sup> , Song Guo<sup>4</sup>, Shengao Jing<sup>1</sup>, Yingjie Li<sup>1</sup>, Cheng Huang<sup>1</sup>, Geoffrey S. Tyndall<sup>2</sup> , John J. Orlando<sup>2</sup>, and Xuan Zhang<sup>5</sup> 

<sup>1</sup>State Environmental Protection Key Laboratory of Formation and Prevention of Urban Air Pollution Complex, Shanghai Academy of Environmental Sciences, Shanghai, China, <sup>2</sup>Atmospheric Chemistry Observation and Modeling Laboratory, National Center for Atmospheric Research, Boulder, CO, USA, <sup>3</sup>Department of Atmospheric Sciences, Texas A&M University, College Station, TX, USA, <sup>4</sup>State Key Joint Laboratory of Environmental Simulation and Pollution Control, College of Environmental Sciences and Engineering, Peking University, Beijing, China, <sup>5</sup>Department of Life and Environmental Sciences, University of California, Merced, CA, USA

**Abstract** We present the analysis of the atmospheric budget of nitrophenols and nitrocresols, a class of nitroaromatics that raise great ecosystem and health concerns due to their phytotoxic and genotoxic properties, during the spring wheat harvest season in Eastern China. Significant quantities with maximum concentrations over 100 pptv and distinct diurnal patterns that peak around midnight and maintain low levels throughout the day were observed, in coincidence with the extensive open crop residue burning activities conducted in the vicinity. An observationally constrained zero-dimension box model was constructed to assess the relative importance of various production and removal pathways at play in determining the measured surface concentrations. The NO<sub>3</sub>-initiated dark chemistry, in concert with meteorological variations predominantly dilution and entrainment, exerts major controls over the observed diurnal behaviors of nitrophenols and nitrocresols. Structural isomerism is predicted to have a significant impact on the multiphase partitioning and chemistry of nitrophenol isomers. Furthermore, simulations show that an appreciable amount of nitrophenols is present in the aerosol water, thereby representing an important source of water-soluble brown carbon in atmospheric aerosols under the humid subtropical weather prevailing during the campaign. Sensitivity analysis performed on the model parameterizations of reaction schemes helps to further understand the chemistry underlying the diurnal cycles. Implementing NO-dependent yields of cresols from toluene photooxidation improves the model predictions of nitrocresols at low NO ranges (<1 ppb), thereby underscoring the complexity of the peroxy radical reaction pathways from toluene photooxidation under atmospheric relevant conditions.

**Plain Language Summary** Nitrophenols and nitrocresols represent an important class of nitroaromatics that impact Earth's climate by contributing to the formation of light-absorbing aerosols (brown carbon). Here, through a combination of field observations and model simulations, we examine the atmospheric transformation mechanisms of nitrophenols and nitrocresols present in large quantities from the open crop residue burning during the spring wheat harvest season in Eastern China. We show that the observed distinct diurnal patterns of nitrophenols and nitrocresols are responsive to the complex interplay of meteorological variations, oxidative processes, and multiphase chemistry in the atmosphere. Our analysis affords insights into the atmospheric life cycle of nitrophenols and nitrocresols with respect to chemical transformation, mass transport, and phase transitions. Such information is essential in further understanding the climate and health consequences of nitrophenols and nitrocresols.

## 1. Introduction

Nitrophenols and nitrocresols have been of environmental and human health concern over the last few decades due to their phytotoxicity that contributes to the forest decline and their genotoxicity that is associated with an increased risk of cancer (Bonney et al., 2012; Rippen et al., 1987). Sources of atmospheric nitrophenols and nitrocresols include direct emissions that result from coal and wood combustion, fugitive emissions in the manufacture of dyes, resins, explosives, and pharmaceuticals, as well as secondary production from the atmospheric nitration processes (Harrison, Barra, et al., 2005). Gas phase production pathways

**Writing – review & editing:** Hongli Wang, Geoffrey S. Tyndall, John J. Orlando, Xuan Zhang

mainly include photooxidation of phenol and cresols in the presence of  $\text{NO}_x$  and the  $\text{NO}_3$ -initiated oxidation of phenol and cresols. In addition, aqueous phase photonitration has been found to contribute to the formation of nitrophenols and nitrocresols as well, the importance of which depends on the abundance of the liquid water content (Harrison, Heal, et al., 2005; Vione et al., 2009).

Once released to the atmosphere, nitrophenols and nitrocresols are subject to degradation that is primarily initiated by reactions with OH radicals during the day and  $\text{NO}_3$  radicals at night. Additionally, nitrophenols and nitrocresols are readily photolyzed due to their strong ultraviolet-visible absorptivity (Chen et al., 2011; Jacobson, 1999). Owing to the presence of strong intramolecular hydrogen bonds between the  $-\text{OH}$  and  $-\text{NO}_2$  moieties, photolysis of nitrophenols and nitrocresols over the 300–500 nm region is a proposed photolytic source of nitrous acid (HONO), an important precursor of OH radicals in the polluted environment (Bejan et al., 2006; Sangwan & Zhu, 2016). Another fate of nitrophenols and nitrocresols in the atmosphere is condensing onto aqueous/organic aerosols and cloud droplets leading to the formation of secondary organic aerosols (SOA). The deprotonated forms of nitrophenols and nitrocresols in the condensed phase are characterized by even stronger absorption at longer wavelengths (Laskin et al., 2015). It has been suggested that nitroaromatics as a group formed through atmospheric oxidation of biomass burning emissions are major chromophores that contribute to the formation of atmospheric brown carbon (Desyaterik et al., 2013; Iinuma et al., 2010; Kitanovski et al., 2012). Further aqueous phase processes, including oxidation by  $\text{OH}_{(\text{aq})}$  and  $\text{NO}_{3(\text{aq})}$  radicals and subsequent nitration to form dinitrophenols, have been suggested as a potential loss pathway of nitrophenols (Vione et al., 2001).

In this work, ground-based measurements of a suite of trace gases were used alongside an observationally constrained zero-dimensional photochemical box model to explore the atmospheric transformation mechanisms of nitrophenols and nitrocresols during the widespread open crop residue burning season in Eastern China. From a series of sensitivity and budget analyses, processes that control the temporal variations of nitrophenols and nitrocresols are identified. By validating the model performance against observations on site, the representativeness of the physicochemical schemes embedded in the model framework is further probed. This work provides an observationally based demonstration of how the interplay of nighttime production, daytime photolysis, boundary layer entrainment, and dilution by ventilation exerts a primary control over the evolution of nitrophenols and nitrocresols in the atmosphere.

## 2. Methods

### 2.1. The EXPLORE-YRD Campaign

The EXPLORE-YRD (EXperiment on the eLucidation of the atmospheric Oxidation capacity and aerosol foRmation and their Effects in Yangtze River Delta) campaign was carried out in the late spring of 2018 (23 May to 24 June) at the Jiangsu Provincial Taizhou weather radar station located in Eastern China ( $32.558^\circ\text{N}$ ,  $119.994^\circ\text{E}$ ). This rural site is surrounded by farmlands and approximately 800 m away from two expressways crossing to the southwest. During the campaign, meteorological conditions were relatively warm ( $T_{\text{avg}} = \sim 295$  K) and humid ( $\text{RH}_{\text{avg}} = \sim 73\%$ ) with frequent sunshine and low wind speed ( $\text{WS}_{\text{avg}} = 2.01$  m/s); see Figure S1 in the supporting information.

### 2.2. Measurements

A suite of instruments was used to measure primary gas pollutants including  $\text{NO}_x$  (Model 42i, Thermo Fischer, USA),  $\text{O}_3$  (Model 49i, Thermo Fischer, USA), CO (Model 48i, Thermo Fischer, USA), and  $\text{SO}_2$  (Model 43C, Thermo Fischer, USA). The photolysis frequencies of  $\text{O}_3$ ,  $\text{NO}_2$ ,  $\text{NO}_3$ , HONO, HCHO, and  $\text{H}_2\text{O}_2$  were calculated from the spectral actinic flux density measured by a customized spectral radiometer (Bohn et al., 2008). Particle size distribution and number concentration were measured by a differential mobility analyzer (Model 3081, TSI, USA) coupled to a condensation particle counter (Model 3787, TSI, USA). The aerosol water content was derived from the measurements of a customized hygroscopicity tandem differential mobility analyzer; see details given in Jing et al. (2016). Organic carbon (OC) and elemental carbon (EC) in fine particles were measured hourly by a semicontinuous analyzer manufactured by Sunset Laboratory Inc; see details given in Hu et al. (2012).

Real-time analysis of nonmethane organic carbons (NMOCs) was performed by a commercial proton transfer reaction time of flight mass spectrometer (PTR-MS, IONICON Analytik GmbH, Austria). Measurements

reported here were obtained at a sampling rate of 0.1 Hz. The instrument was operated in the  $m/z$  range of 0 to 530, with a mass resolution in the range of 3,500 to 5,500 at  $m/z$  45–204. The drift tube was operated at 850 V with a pressure of 3.8 mbar at 80°C. Calibrations were performed by gas standards (Spectra Gases Inc. USA) and certified permeation tubes (KinTek Inc. USA) at five concentration levels from 0 to 10 ppbv. The calibration mixture includes formic acid ( $\text{CH}_2\text{O}_2$ ), acetic acid ( $\text{C}_2\text{H}_4\text{O}_2$ ), furan ( $\text{C}_4\text{H}_4\text{O}$ ), acrylic acid ( $\text{C}_3\text{H}_4\text{O}_2$ ), propionic acid ( $\text{C}_3\text{H}_6\text{O}_2$ ), butyric acid ( $\text{C}_4\text{H}_8\text{O}_2$ ), furfural ( $\text{C}_5\text{H}_4\text{O}_2$ ), phenol ( $\text{C}_6\text{H}_6\text{O}$ ), *o*-cresol ( $\text{C}_7\text{H}_8\text{O}$ ), 4-nitrophenol ( $\text{C}_6\text{H}_5\text{NO}_3$ ), 3-methyl-4-nitrophenol ( $\text{C}_7\text{H}_7\text{NO}_3$ ), benzaldehyde ( $\text{C}_7\text{H}_6\text{O}$ ), naphthalene ( $\text{C}_{10}\text{H}_8$ ), and limonene ( $\text{C}_{10}\text{H}_{16}$ ). Sensitivity of all standards tested here is in the range of 745 to 3,176 ncps/ppbv; see details in Table S1 in the supporting information. Although phenol and *o*-cresol were included in the calibration mixture, it is known that PTR-MS measurements of phenol and cresols can suffer mass interferences from fragmentation of larger organics (Jobson et al., 2011) and we note that the phenol and cresols measurements were not used in this study.

A custom-built online gas chromatography system equipped with a mass spectrometer and a flame ionization detector (GC-MS/FID) was used to measure  $\text{C}_2$ – $\text{C}_{10}$  hydrocarbons and halocarbons with a time resolution of 1 hr. Most  $\text{C}_2$ – $\text{C}_5$  hydrocarbons were measured by the FID channel equipped with a PLOT column (15 m  $\times$  0.32 mm ID, J&W Scientific, USA). Other compounds were analyzed by the MS channel using a DB-624 column (30 m  $\times$  0.25 mm ID, J&W Scientific, USA). Single point calibrations were performed on a daily basis with a mixture of gas standards at the concentration of 1 ppbv. Detailed description of the system can be found in Liu et al. (2009). Comparison of GC measured acetonitrile and a selection of VOCs relevant to this study with the corresponding PTR-MS measurements was conducted, and agreement within ~19% was achieved.

### 2.3. Modeling

The 0-D box model (Wang et al., 2019) used for simulating the diurnal profiles of species of interest accounts for (i) gas phase daytime and nighttime chemistry, (ii) dynamic partitioning within gas, liquid, and particle phases, (iii) emission, (iv) dry deposition, (v) dilution, and (vi) entrainment of background air from the free troposphere. A conservation balance on  $C_g^i$ , the gas phase concentration of a given compound  $i$ , is expressed as follows:

$$\frac{dC_g^i}{dt} = P_{chem,i} - L_{chem,i} + \left(\frac{dC_g^i}{dt}\right)_{gp} + \left(\frac{dC_g^i}{dt}\right)_{gaq} + E_i - k_{dep,i}C_g^i - k_{dil,i}C_g^i - k_{ent,i}(C_g^i - C_{bkg}^i) \quad (1)$$

where  $P_{chem,i}$  and  $L_{chem,i}$  are the production and removal rates with respect to gas phase chemistry, the two differential terms,  $(dC_g^i/dt)_{gp}$  and  $(dC_g^i/dt)_{gaq}$ , represent the gas-particle partitioning and the mass transfer between the gas and liquid phase, respectively,  $E_i$  is the emission rate,  $k_{dep,i}$  is the dry deposition rate coefficient, which is calculated using the industrial source complex model system (Atkinson et al., 1997),  $k_{dil,i}$  is the first-order dilution rate coefficient that characterizes transport processes such as mixing of outside air and is constrained by the measured diurnal variations of acetonitrile (Figure S2 in the supporting information),  $C_{bkg}^i$  is the concentration of species  $i$  in the residual layer, which is assumed as zero, and  $k_{ent,i}$  is the rate coefficient for entrainment:

$$k_{ent,i} = \frac{dH}{dt} \frac{1}{H} \quad \text{if } \frac{dH}{dt} > 0 \quad k_{ent,i} = 0 \quad \text{if } \frac{dH}{dt} \leq 0 \quad (2)$$

where  $H$  is the boundary layer height, which is derived from the European Centre for Medium-Range Weather Forecasts (ECMWF) reanalysis data (ERA5 hourly data, accessible at <https://cds.climate.copernicus.eu/cdsapp#!/dataset/reanalysis-era5-single-levels?tab=overview>).

Reaction kinetics and mechanisms for the gas phase degradation of major VOCs observed during the campaign, including propylene, acrolein, furan, isoprene, benzene, toluene, and monoterpenes, were extracted from the Master Chemical Mechanism (MCMv3.3.1, accessible at <http://mcm.leeds.ac.uk/MCM/>). Photolysis kinetics of nitrophenols and nitrocresols derived from previous studies (Bardini, 2006; Chen et al., 2011) were added into the gas phase scheme; see Table S2 in the supporting information. In addition to gas phase reactions, a simplified scheme describing the production of nitrophenols from the aqueous

nitration of phenol was incorporated in the model as well; see reactions listed in Table S2 in the supporting information. Kinetics for the sequential reactions of phenol with OH and NO<sub>2</sub> are derived from measurements by Barzaghi and Herrmann (2002).

The gas-particle partitioning of a given species *i* is treated as a dynamic mass transfer process:

$$\left(\frac{dC_g^i}{dt}\right)_{gp} = -k_{gp,i}C_g^i + k_{pg,i}C_p^i \quad (3)$$

$$\left(\frac{dC_p^i}{dt}\right)_{pg} = k_{gp,i}C_g^i - k_{pg,i}C_p^i \quad (4)$$

where  $C_p^i$  is the particle phase concentration of species *i* and  $k_{gp,i}$  and  $k_{pg,i}$  are first-order rate constants for species *i* transport to and from aerosols. As the gas-particle mass transfer can be limited by gas phase diffusion, interfacial uptake and bulk phase diffusion, we use the gas-particle accommodation coefficient,  $\alpha_{p,i}$ , to approximate resistances to gas-particle partitioning from interface accommodation and particle phase diffusion (Cappa et al., 2013; Huang et al., 2018; McVay et al., 2016; Zhang et al., 2015). Thus, the overall rate constant from gas to aerosol phase  $k_{gp,i}$  can be expressed as follows:

$$\frac{1}{k_{gp,i}} = \frac{1}{4\pi D_{g,i} R_p N_p} + \frac{1}{\pi \alpha_{p,i} \bar{c}_i R_p^2 N_p} \quad (5)$$

where  $D_{g,i}$  is the gas phase diffusivity of species *i*,  $\bar{c}_i$  is the gas phase mean velocity of species *i*,  $R_p$  is the particle radius, and  $N_p$  is the number of particles per unit volume of air. In the model, a single particle size bin of 100 nm is used, such that the particle number concentration can be calculated based on the measured organic aerosol mass concentration ( $C_{OA}$ ) (Nah et al., 2016; Schwantes, McVay, et al., 2017; Zhang et al., 2014; Zhang & Seinfeld, 2013). The mass transfer between the gas and particle phase is a continuous process till equilibrium is established which is assumed to follow Raoult's law; therefore, the mass transfer from the particle to the gas phase is given by

$$\frac{k_{gp,i}}{k_{pg,i}} = \frac{RT C_{OA}}{P_i M_{OA} \gamma_{OA}} \quad (6)$$

where  $R$  is the ideal gas constant,  $T$  is the temperature,  $P_i$  is the vapor pressure of species *i*,  $M_{OA}$  is the organic aerosol mean molecular weight, and  $\gamma_{OA}$  is the particle phase activity coefficient, which is assumed to be unity here. Note that the value of activity coefficient used in the model does not significantly impact the simulated diurnal profiles; see Figure S3 in the supporting information.

The mass transfer between gas and aqueous phase (aerosol water) is described by a set of mass balance differential equations (Seinfeld & Pandis, 2016), the general form of which, for the species *i* in the gas phase, is given by

$$\left(\frac{dC_g^i}{dt}\right)_{gaq} = -k_{gaq,i} w_A C_g^i + \frac{1}{H_i^*} k_{gaq,i} w_A C_{aq}^i \quad (7)$$

where  $w_A$  is the aerosol liquid water volume fraction, which is derived from the aerosol water content measurements,  $H_i^*$  is the effective Henry's law constant,  $C_{aq}^i$  is the corresponding concentration of species *i* in the aqueous phase, and  $k_{gaq,i}$  is the mass transfer coefficient for gas phase plus interfacial mass transport, given by:

$$\frac{1}{k_{gaq,i}} = \frac{R_{aq}^2}{3D_{g,i}} + \frac{4R_{aq}}{3\alpha_{aq,i}\bar{c}_i} \quad (8)$$

where  $\alpha_{aq,i}$  is the gas aqueous accommodation coefficient for species *i* and  $R_{aq}$  is the radius of the aqueous aerosol, which is calculated based on the in situ measurements of the aerosol water content assuming the

same amount of water is represented by one single liquid particle. Assuming identical size distributions as organic aerosols, the correlation of  $R_{\text{aq}}$  with  $R_{\text{p}}$  can be obtained based on the measurements of organic aerosol mass concentration and aerosol water content. Values of parameters describing the multiphase mass transfer processes are given in Table S3 in the supporting information.

The model was driven with in situ measured temperature, relative humidity, and pressure, as well as the boundary layer height derived from ECMWF reanalysis data. Prior to each simulation, a 24 hr spin-up period was applied. The model was run in 10 min steps, and for each time step, the mass balance equation of any given NMOC precursor incorporated in the model read in the instantaneously measured values. The simulated concentrations of CO, NO<sub>x</sub>, O<sub>3</sub>, and HCHO are constrained to real-time measurements. The photolysis frequencies ( $J$ ) of O<sub>3</sub>, NO<sub>2</sub>, NO<sub>3</sub>, HONO, HCHO, and H<sub>2</sub>O<sub>2</sub> were constrained to real-time measurements as well, and the  $J$  values of other species were scaled to  $J_{\text{NO}_2}$ . As described later, detailed analyses were conducted on the freshest plume observed at the site, to essentially eliminate the effects of atmospheric aging on the measurements and their interpretation.

### 3. Results and Discussions

#### 3.1. Identification of Biomass Burning Plumes

Acetonitrile is a common biomass burning tracer that has been used to identify air parcels intercepted by fire plumes (Coggon et al., 2016; De Gouw et al., 2003). As shown in Figure 1, periods with biomass burning impact are readily distinguished by the intense pulses of acetonitrile, together with benzene, toluene, furan, and furfural, a group of aromatics that exhibit strong positive correlation with acetonitrile. Furan and its derivatives have been suggested as potential biomass burning tracers due to their significant enhancement in fire plumes and relatively negligible emissions from primary urban and natural sources (Gilman et al., 2015). A distinct diurnal pattern of selected tracers is observed during the campaign with a relatively small day-to-day variability: A sharp peak appears around midnight and decreases fairly continuously after the peak.

Organic species with average levels exceeding 1 ppb primarily comprise of small acids, alcohols, carbonyls, and aromatic hydrocarbons. Their observed enhancement ratios (ERs) over background levels relative to the acetonitrile enhancement ( $\Delta X/\Delta \text{ACN}$ ) observed after midnight are given in Figure 1b, along with the literature reported ERs obtained from laboratory-based burns of a few types of wheat straw (WS). Molecular formulas interpreted from PTR-MS measurements, which are often likely composed of more than one species, are given here for comparison purposes. In general, the ERs of species measured in the present study, particularly CH<sub>4</sub>O (methanol) and C<sub>3</sub>H<sub>6</sub>O (the mixture of acetone and propanal), appear reasonably close to the ERs derived from burning dry wheat straw residues under smoldering-dominant conditions. This is in fact not surprising as late spring is the wheat harvest season in the Yangtze River Delta region, and large-scale burn typically occurs in May and June (Kudo et al., 2014). Note that wheat grown in different geographic locations, whether China (CHN) or United States (US), yields similar ERs upon burning. Toluene has slightly higher ERs compared with those measured from all types of wheat straw burn, suggesting that the OH-initiated chemistry is inappreciable in the fire plumes observed. One exception is C<sub>5</sub>H<sub>8</sub> (isoprene), the ER of which is lower by a factor of 1.5 on average compared with that derived from fresh plumes of burning wheat straw residues. This is due to the high reactivity of isoprene toward NO<sub>3</sub> radicals generated in the nighttime fire plumes (Wennberg et al., 2018). Other NO<sub>3</sub>-consuming molecules, such as C<sub>2</sub>H<sub>4</sub>O (acetaldehyde) and C<sub>4</sub>H<sub>6</sub>O (methacrolein and methyl vinyl ketone), exhibit different degrees of reduced ERs as well. The extent to which the plumes encountered at the sampling site are processed in transit can be evaluated by calculating the amount of isoprene reacted during the transport of the fire plumes. For the following discussions, we choose the fresh fire plume to explore the atmospheric transformation mechanism of nitrophenols and nitrocresols upon emissions.

#### 3.2. Sources and Sinks of Nitrophenols and Nitrocresols

Figure 2 depicts the diurnal trends of nitrophenols and nitrocresols observed on 24 May, when the maximum levels were measured for both compounds during the campaign. A sharp increase is usually observed after midnight, peaking around 4:00 local time, and then decays away by the early morning and maintains relatively low levels throughout the day. By the late evening, a second peak appears, the intensity of which is

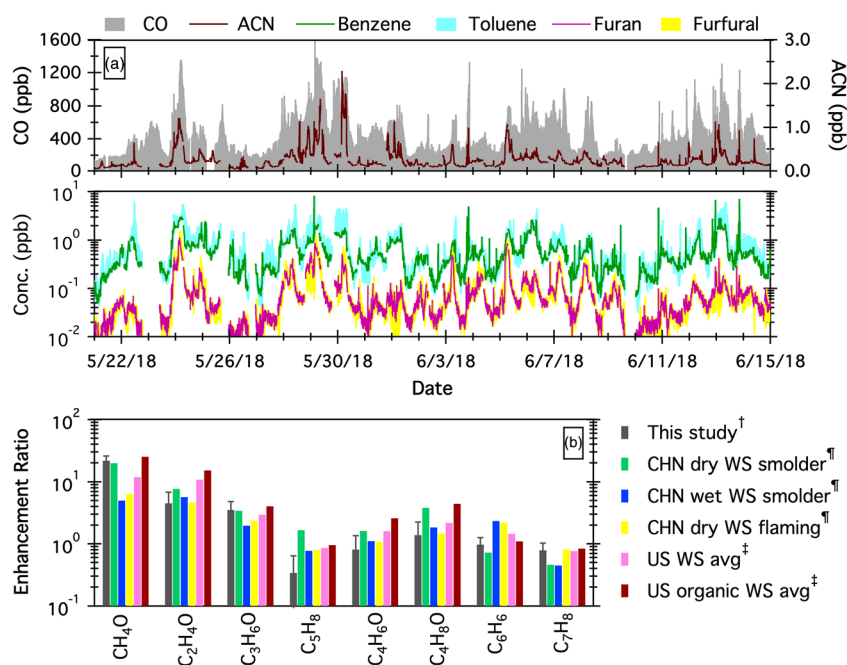


**Figure 1.** (a) Temporal profiles of CO, acetonitrile (ACN), benzene, toluene, furan and furfural observed during the campaign and (b) enhancement ratios (ERs) of selected species, including CH<sub>4</sub>O (methanol), C<sub>2</sub>H<sub>4</sub>O (acetaldehyde), C<sub>3</sub>H<sub>6</sub>O (acetone and propanal), C<sub>3</sub>H<sub>8</sub> (isoprene), C<sub>4</sub>H<sub>6</sub>O (methacrolein and methyl vinyl ketone), C<sub>4</sub>H<sub>8</sub>O (butanal and methyl ethyl ketone), C<sub>6</sub>H<sub>6</sub> (benzene), and C<sub>7</sub>H<sub>8</sub> (toluene), to acetonitrile averaged over six time periods when intensive acetonitrile emissions were observed (05/24, 05/29, 05/30, 06/01, 06/03, and 06/05)<sup>†</sup>. Also given are literature reported ERs from burning of wheat straw (WS) and organic wheat straw grown in the United States (Stockwell et al., 2015)<sup>‡</sup>, as well as Chinese (CHN) dry and wet wheat straw residues burnt under flaming-dominant versus smoldering-dominant conditions (Inomata et al., 2015)<sup>¶</sup>. Note that the reported ERs of C<sub>5</sub>H<sub>8</sub> by Inomata et al. (2015) have potential C<sub>4</sub>H<sub>4</sub>O (furan) interferences.

approximately half of the first pulse. The average concentration of nitrophenols observed here is 46.4 ppt (max = 121.7 ppt), higher than the reported gas phase range (0.02–56 ppt) measured in other geographic locations (Belloli et al., 1999; Leuenberger et al., 1988; Lüttke et al., 1999; Yuan et al., 2016). Also given in Figure 2 are the simulated temporal profiles of nitrophenols and nitrocresols, showing reasonable agreement with the measurements. Additional simulations and comparison with observed diurnal patterns during persistent biomass burning scenarios are given in Figure S4 in the supporting information.

The observed diurnal variation of nitrophenols and nitrocresols is a result of intertwined processes, including emissions, physical losses, and photochemical production and removal, the relative importance of which is further probed here. As a biomass burning tracer with negligible chemical reactivity in the atmosphere, acetonitrile serves as an observational constraint for quantifying the combined effect of emission and dilution. The emission rates of phenol and cresols as precursors of nitrophenols and nitrocresols, respectively, are determined based on their ERs relative to acetonitrile ( $\Delta\text{PHE}/\Delta\text{ACN} = 0.887$  and  $\Delta\text{CRE}/\Delta\text{ACN} = 0.661$ ) derived from standard dry wheat straw burning (Stockwell et al., 2015). It is worth noting that these prescribed emission ratios would have resulted in an overestimation of nitrocresols if any rapid oxidation process occurred prior to the detection of the plume because cresols are much more reactive toward OH and NO<sub>3</sub> than phenol. Nevertheless, as the measured ER of isoprene to acetonitrile indicates that the plume examined here is rather fresh ( $\Delta\text{ISOP}/\Delta\text{ACN} = 0.73$  compared with  $0.84 \pm 0.11$  derived from laboratory measurements), the uncertainties associated with the emissions of nitrophenols and nitrocresols due to atmospheric aging prior to their detection are likely low.

As shown in Figure 2, nitrophenols and nitrocresols exhibit very similar diurnal patterns; we will hereby use nitrophenols as an illustration for a detailed budget analysis. The pulse of nitrophenols appearing at ~04:00–05:00 local time is largely from the NO<sub>3</sub>-initiated oxidation of primary phenol emissions. The chemical removal of nitrophenols at night is minor, while dilution by ventilation leads to a rapid decline of

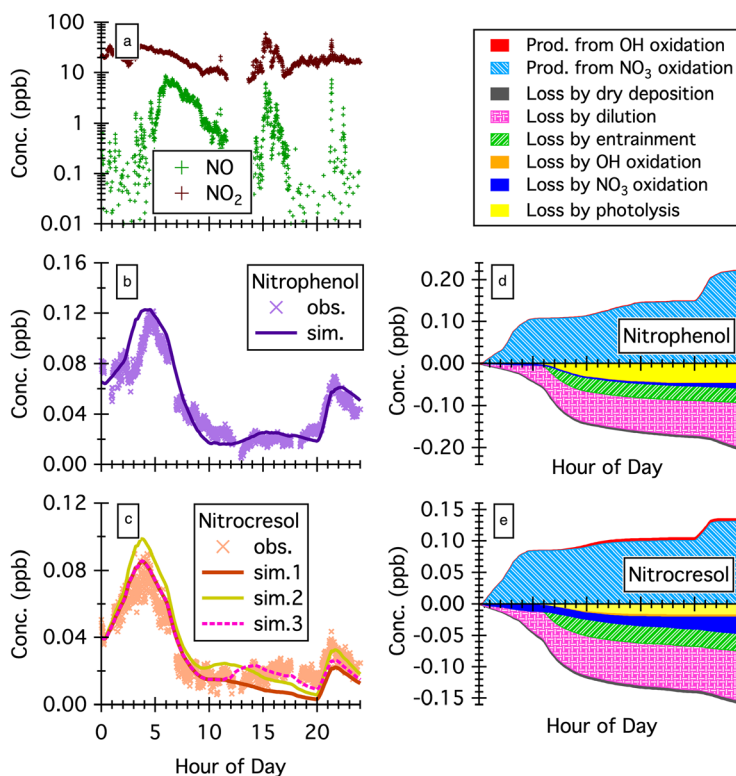


**Figure 2.** (a) Diurnal profiles of NO<sub>x</sub> on 24 May, when maximum levels of nitrophenols and nitrocresols were observed throughout the campaign. (b) Simulated (sim.) and observed (obs.) diurnal variations of nitrophenols (NP). (c) Simulated (sim.1: based case; sim.2: increasing reaction rates of methyl phenoxy radicals with NO<sub>2</sub>; sim.3: NO-dependent yield of cresols from OH-oxidation of toluene) and observed (obs.) diurnal variations of nitrocresols (NC). (d) Contribution of different production and removal processes, including OH-initiated oxidation of benzene and phenol, NO<sub>3</sub>-initiated oxidation of phenol, OH- and NO<sub>3</sub>-initiated oxidation of nitrophenols, photolysis of nitrophenols, dilution, dry deposition, and entrainment, to the daily budget of nitrophenols. (e) Contribution of different production and removal processes to the daily budget of nitrocresols. Rates of individual processes are given in Figure S5 in the supporting information.

nitrophenols before dawn (Figure 2d). By the time of sunrise (~06:00), the mixed layer depth starts to increase, further reducing the concentration by ~46%. The simulated turnover in the early morning (~09:00–10:00) is particularly sensitive to the ascending rate of the boundary layer height. The level of nitrophenols remains rather constant throughout the day, and no obvious increase is observed with the onset of photochemistry. The production of nitrophenols from sequential benzene oxidation is well balanced by the photochemical loss that is driven predominantly by photolysis. A series of sensitivity analysis is further performed to evaluate the role of daytime and nighttime chemistry in modulating the dynamics of nitrophenols and nitrocresols. The NO<sub>3</sub>-initiated oxidation as both production and removal pathways exerts primary control over the simulated profiles. For example, increasing the reaction rates of nitrophenols and nitrocresols with NO<sub>3</sub> by a factor of 10 reduces the simulated average concentrations by ~30% and ~50%, respectively; see Figure S6 in the supporting information. Photolysis constitutes an important removal channel of nitrophenols, but less effective on nitrocresols, the average photolysis rate of which is nearly 1 order of magnitude lower than that of nitrophenols (Bejan et al., 2007). Variations in the photolysis rates of nitrophenols and nitrocresols by an order of magnitude lead to changes in the simulated average daytime concentrations by ~80% and ~20%, respectively. The OH-initiated oxidation chemistry, either as production or loss pathways, does not remarkably affect the simulated diurnal trends of nitrophenols and nitrocresols.

While the simulated diurnal profile of nitrophenols reasonably matches the observations throughout the day, the nitrocresols simulation, on the other hand, starts to deviate low from the measured trend in the mid-afternoon (~LT 15:00). By the time the second peak appears (~LT 21:00), the predicted nitrocresols level only

accounts for a third of the measurement (Sim.1 in Figure 2c). Such an underprediction occurs during the transition from OH oxidation to NO<sub>3</sub> oxidation dominated chemical regime. Varying the NO<sub>3</sub> concentration by adjusting the reactive uptake coefficient of N<sub>2</sub>O<sub>5</sub> on aerosols (in the range of 0.001–0.05 and a value of 0.02 [Evans & Jacob, 2005] is used as default) and consequently the sink of NO<sub>3</sub> does not significantly improve this underprediction as NO<sub>3</sub> acts as both a source and a sink of nitroresols. The NO<sub>3</sub>-initiated oxidation of cresols has been postulated to proceed via an overall H-atom abstraction mechanism that occurs after ring addition of NO<sub>3</sub> to form methyl phenoxy radicals, which further react with NO<sub>2</sub> to form nitroresol isomers (Bolzacchini et al., 2001; Olariu et al., 2013). While increasing the reaction rate of methyl phenoxy radicals with NO<sub>2</sub> by a factor of 3 could certainly lead to an enhanced production of nitroresols and thereby better model-measurement agreement at LT ~ 21:00–23:00, the model predictions during the first pulse at LT ~ 04:00–05:00, however, would be inherently biased high (Sim.2 in Figure 2c). Another hypothesis with the potential to explain the model-measurement discrepancy is the varying yield of cresols as a function of NO levels from toluene photooxidation, as opposed to a fixed value of 18% across all NO conditions as in the current MCMv3.3.1 scheme embedded in the model. Indeed, the observed molar yield of cresols ( $Y = 39 \pm 5\%$ ) in the absence of NO<sub>x</sub> by Ji et al. (2017) is more than twice of the measurements conducted under high NO<sub>x</sub> conditions (Klotz et al., 1998; Schwantes, Schilling, et al., 2017; Smith et al., 1998). Birdsall et al. (2010) have found that the addition of NO to the toluene oxidation system could suppress the yield of cresols by up to 30%. By parameterizing the NO-dependent yield of cresols in the model scheme (see details in Table S4 in the supporting information), the predicted levels of nitroresols could match the observations in the early evening (Sim.3 in Figure 2c) when the NO level was below 1 ppbv (Figure 2a). The hypothesis of NO-dependent yield of cresols from toluene photochemistry warrants further experimental investigation, which is out of the scope of the current study.

### 3.3. Multiphase Chemistry of Isomer Resolved Nitrophenols and Nitroresols

Nitrophenol isomers, including 2-nitrophenol and 4-nitrophenol, are produced from the reaction of NO<sub>2</sub> with the phenoxy radical, which stems from the abstraction of phenol by either OH or NO<sub>3</sub> (Atkinson et al., 1992). While OH-initiated oxidation of phenol only generates a small amount of 2-nitrophenol (~6%), both 2-nitrophenol and 4-nitrophenol have been observed through the NO<sub>3</sub>-oxidation pathway, with molar yields of ~24% and ~50%, respectively (Olariu et al., 2002). Interestingly, structural isomerism, particularly positional isomerism, has a significant impact on both volatility and water solubility of nitrophenol isomers: The vapor pressure and Henry's law constant of 4-nitrophenol at 298 K are  $6.6 \times 10^{-7}$  atm and  $3.0 \times 10^5$  M atm<sup>-1</sup>, respectively, differing by at least 2 orders of magnitude from 2-nitrophenol ( $P_{2NP} = 1.5 \times 10^{-4}$  atm and  $H_{2NP} = 81.1$  M atm<sup>-1</sup>) (Sander, 2015; Scala & Banerjee, 1982). As shown in Figure 3a, an appreciable fraction of modeled nitrophenols (up to ~30%) was found in the aerosol water predominantly in the form of the 4-nitrophenol isomer. Despite the large difference in the vapor pressure of the two isomers, their total fraction in the particle phase (in the range of  $4.8 \times 10^{-5}$ – $1.2 \times 10^{-2}$ ) is still negligible compared with the gas phase level. Yuan et al. (2016) calculated that the particle phase fraction of nitrophenol isomers originating predominantly from secondary production is on average ~0.053, much higher than the present study, primarily owing to the low temperature ( $-5 \pm 5^\circ\text{C}$ ) prevailing during their campaign conducted in winter. The varying degrees of multiphase partitioning of nitrophenol isomers can explain a number of previous measurements showing that 4-nitrophenol is the dominant isomer in cloud water while the majority of 2-nitrophenol remains in the gas phase (Leuenberger et al., 1988; Levsen et al., 1993; Lüttke et al., 1999). A number of nitroresol isomers, including 3-methyl-2-nitrophenol, 3-methyl-4-nitrophenol, 4-methyl-2-nitrophenol, 5-methyl-2-nitrophenol, and 6-methyl-2-nitrophenol, have been observed as products of OH/NO<sub>3</sub>-initiated oxidation of toluene in the presence of NO<sub>x</sub> (Atkinson et al., 1992; Grosjean, 1984; Olariu et al., 2002, 2013). In contrast to nitrophenols, the effect of structural isomerism on the volatility of nitroresol isomers is inappreciable (Dang et al., 2019). The fraction of all nitroresol isomers in organic aerosols ( $6.0 \times 10^{-3}$ – $1.5 \times 10^{-2}$ ) is slightly higher than nitrophenols due to the presence of an additional methyl group that lowers the volatility. The water solubility of 3-methyl-4-nitrophenol ( $H_{3M4N} = 6.8 \times 10^4$  M atm<sup>-1</sup>) is approximately 2–3 orders of magnitude higher than all the other isomers, accounting for over 99% of the total nitroresol isomers in the aerosol water, though still negligible compared with the gas phase levels; see Figure 3a.

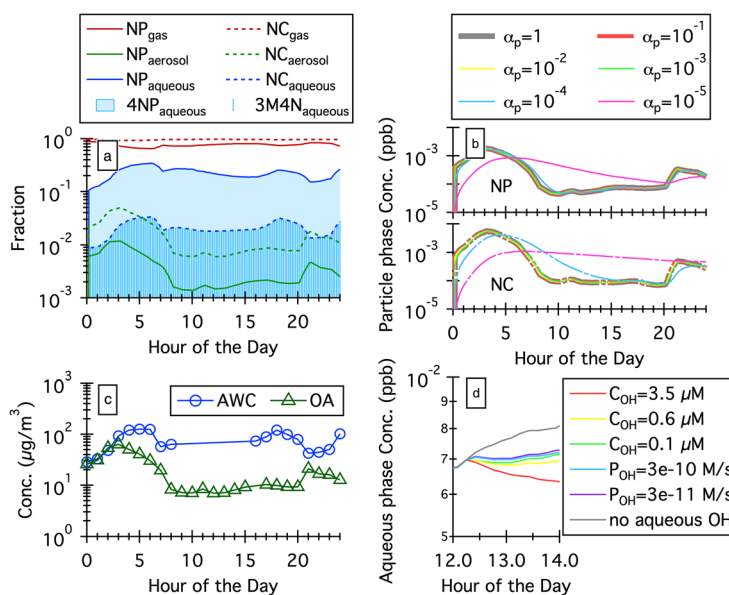


**Figure 3.** (a) Fraction of nitrophenols (NP) and nitrocresols (NC) in the gas, particle and aqueous phases. Also given are the aqueous phase fractions of 4-nitrophenol (4NP) and 3-methyl-4-nitrophenol (3M4N) as dominant isomers. (b) Diurnal trends of particle phase nitrophenols and nitrocresols under a range of gas-particle mass transfer resistances represented by the accommodation coefficient ( $\alpha_p$ ). (c) Measured concentrations of aerosol water content (AWC) and organic aerosols (OA) that are used for simulating the multiphase mass transfer of nitrophenols and nitrocresols. (d) The effect of aqueous phase nitration chemistry on the level of nitrophenols in aerosol water at noon (12:00–14:00 LT). The aqueous phase OH radicals are either produced at a rate of  $P_{\text{OH}} = (0.3\text{--}3) \times 10^{-10} \text{ M s}^{-1}$  or remain constant as  $C_{\text{OH}} = 0.1\text{--}3.5 \mu\text{M}$ .

The effect of aerosol physical state on the simulated profiles of nitrophenols and nitrocresols is probed by varying the accommodation coefficient ( $\alpha_p$ ), a parameter that approximates mass transfer resistances resulting from both interface accommodation and bulk phase diffusion. Low  $\alpha_p$  values characterize an amorphous semisolid particle phase that can kinetically inhibit the mass transfer of nitrophenols and nitrocresols, whereas  $\alpha_p$  of unity is characteristic of quasi-instantaneous gas-particle partitioning (Huang et al., 2016; Krechmer et al., 2015; Zhang et al., 2014). As shown in Figure 3b, increasing  $\alpha_p$  from  $10^{-5}$  to 1 leads to enhanced partitioning of nitrophenols and nitrocresols to the aerosol phase by a factor of 1.6 and 4.3 on average, respectively. In addition, the characteristic timescale for establishing partitioning equilibrium decreases from 58 days to 86 s for nitrophenols and 62 days to 92 s for nitrocresols, thereby yielding a particle phase temporal profile that resembles the observed gas phase diurnal pattern. Overall, the treatment of gas-particle partitioning (retarded vs. instantaneous equilibration) does not significantly impact the simulated gas phase concentrations of nitrophenols and nitrocresols.

A series of sensitivity tests were also performed to assess the role of aqueous phase nitration processes in the formation of nitrophenols. A simplified reaction scheme that involves a sequential reaction of phenol<sub>(aq)</sub> with OH<sub>(aq)</sub> and NO<sub>2(aq)</sub> is incorporated into the model (Barzagli & Herrmann, 2002, 2004; Harrison, Heal, et al., 2005). In the scheme, OH radicals in the aerosol water are either generated with a daytime production rate of  $(0.3\text{--}3) \times 10^{-10} \text{ M s}^{-1}$  (Arakaki & Faust, 1998; Bianco et al., 2015; Wang et al., 2012; Zhang et al., 2009) or remain constant in the range of 0.1–3.5  $\mu\text{M}$ , a substantially high level that is likely present in nascent cloud droplets (Paulson et al., 2019). As shown in Figure 3d, increasing aqueous OH concentrations does not necessarily enhance the production of nitrophenols as the dissolved NO<sub>2(aq)</sub> generated from the photolysis of nitrate and uptake of gas phase NO<sub>2</sub> can be rapidly consumed by hydrolysis and reaction with OH<sub>(aq)</sub> (see detailed reactions listed in Table S2 in the supporting information). As a result, the availability of NO<sub>2(aq)</sub>, which is the essential ingredient for nitrophenols formation, ultimately determines the amount of nitrophenols<sub>(aq)</sub> that can be produced via the aqueous phenol<sub>(aq)</sub> nitration pathway. It is worth noting that an incomplete representation of the kinetics that cascade nitrogen through its different oxidation states in the aqueous phase may introduce large uncertainties to the simulated concentrations of NO<sub>2(aq)</sub>.

Nevertheless, the aqueous phase phenol<sub>(aq)</sub> nitration is shown to account for a minor pathway in the overall nitrophenols production here as the amount of phenol<sub>(aq)</sub> dissolved in the aerosol water is rather limited and the OH-driven degradation does not significantly enhance its effective solubility.

#### 4. Conclusions

With an emerging awareness of the role that nitroaromatics play in brown carbon formation and its climate consequences, understanding the behavior of these chromophores in the atmosphere has become a priority in atmospheric chemistry research. During the EXPLORE-YRD campaign carried out in the late spring of 2018 in Eastern China, significant amounts of nitrophenols and nitrocresols, peaking at ~120 and ~80 ppt, respectively, were observed as a result of large-scale agricultural biomass burning activities during the wheat harvest season. These two nitroaromatics exhibit a distinct diurnal pattern—a sharp peak appears after midnight and then decays away by the early morning and remains low throughout the day until the early evening when the second small peak develops—a pattern that implies the schedule of burning crop residues in the area. These intensive biomass burning events identified in this study release large quantities of air pollutants, including CO (avg. ~863 ppb), NO<sub>x</sub> (avg. ~46 ppb), O<sub>3</sub> (avg. ~98 ppb), and PM<sub>2.5</sub> (avg. ~95 μg/m<sup>3</sup>); see details in Figure S1 in the supporting information, representing one of the major anthropogenic emissions to the local environment.

A 0-D box model that accounts for the complex interplay of meteorological variations and atmospheric oxidative processes was developed to examine mechanistically the role of different factors playing into the atmospheric evolution of nitrophenols and nitrocresols. Processes that govern the diurnal behaviors of these two nitroaromatics were identified, including nighttime oxidation as the predominant production channel and the combination of dilution, entrainment, photolysis, and nighttime oxidation as major removal pathways. Additionally, the majority of the 4-nitrophenol isomer resides in the aerosol water due to its high water solubility, accounting for approximately one third of the total amount of nitrophenols measured in the atmosphere. Therefore, the gas aqueous mass transfer of nitrophenols and their subsequent aqueous phase chemistry, if any, represent an important source of water-soluble brown carbon in atmospheric aerosols under the typical humid subtropical weather prevailing during the campaign.

The comparison of model simulations with measurements allows for the assessment of the extent to which the physicochemical processes incorporated into the model framework are representative of the actual atmospheric conditions. We show that the model adequately captures the diurnal variations of nitrophenols but constantly underpredicts nitrocresols under low to intermediate NO conditions (<1 ppb). From a series of sensitivity analysis, one hypothesis that potentially explains this underprediction is that the yield of cresols from toluene photooxidation is likely NO dependent, and using one fixed yield value derived from experiments conducted in the presence of hundreds of ppb NO might not accurately reflect the reaction pathways at play in the real atmosphere (Zhang et al., 2018). Parameterizing the yield of cresols as a function of NO from toluene photochemistry in the model chemical scheme could help resolve the discrepancy between predictions and measurements. Understanding the behavior of primary peroxy radicals from the OH-initiated oxidation of toluene at a range of atmospheric-relevant NO levels requires additional work.

#### Conflict of Interest

The authors declare no financial or affiliation conflicts of interest.

#### Data Availability Statement

Data presented in this paper are freely accessible from the following link: (<https://data.mendeley.com/datasets/2mpg96mvkb/1>). The box model is based on IGOR Pro and is freely available from the following link (<https://sites.google.com/view/wangsiyuan/models>).

#### References

- Arakaki, T., & Faust, B. C. (1998). Sources, sinks, and mechanisms of hydroxyl radical ( $\bullet$ OH) photoproduction and consumption in authentic acidic continental cloud waters from Whiteface Mountain, New York: The role of the Fe (I) ( $r = \text{II, III}$ ) photochemical cycle. *Journal of Geophysical Research*, 103(D3), 3487–3504. <https://doi.org/10.1029/97JD02795>

#### Acknowledgments

This work is supported by the National Key R&D Program of China (2018YFC0213801) and the Shanghai Science and Technology Commission of the Shanghai Municipality (18QA1403600). The National Center for Atmospheric Research is operated by the University Corporation for Atmospheric Research under the sponsorship of the National Science Foundation.

- Atkinson, D. G., Bailey, D. T., Irwin, J. S., & Touma, J. S. (1997). Improvements to the EPA industrial source complex dispersion model. *Journal of Applied Meteorology*, 36(8), 1088–1095. [https://doi.org/10.1175/1520-0450\(1997\)036<1088:ITTEIS>2.0.CO;2](https://doi.org/10.1175/1520-0450(1997)036<1088:ITTEIS>2.0.CO;2)
- Atkinson, R., Aschmann, S. M., & Arey, J. (1992). Reactions of hydroxyl and nitrogen trioxide radicals with phenol, cresols, and 2-nitrophenol at 296 + –2 K. *Environmental Science & Technology*, 26(7), 1397–1403. <https://doi.org/10.1021/es00031a018>
- Bardini, P. (2006). *Atmospheric chemistry of dimethylphenols & nitrophenols*, PhD (pp. 1–156). Corcaigh: University College Cork.
- Barzaghi, P., & Herrmann, H. (2002). A mechanistic study of the oxidation of phenol by OH/NO<sub>2</sub>/NO<sub>3</sub> in aqueous solution. *Physical Chemistry Chemical Physics*, 4(15), 3669–3675. <https://doi.org/10.1039/b201652d>
- Barzaghi, P., & Herrmann, H. (2004). Kinetics and mechanisms of reactions of the nitrate radical (NO<sub>3</sub>) with substituted phenols in aqueous solution. *Physical Chemistry Chemical Physics*, 6(23), 5379–5388. <https://doi.org/10.1039/b412933d>
- Bejan, I., Barnes, I., Olariu, R., Zhou, S., Wiesen, P., & Benter, T. (2007). Investigations on the gas-phase photolysis and OH radical kinetics of methyl-2-nitrophenols. *Physical Chemistry Chemical Physics*, 9(42), 5686–5692. <https://doi.org/10.1039/b709464g>
- Bejan, I., El Aal, Y. A., Barnes, I., Benter, T., Bohn, B., Wiesen, P., & Kleffmann, J. (2006). The photolysis of ortho-nitrophenols: A new gas phase source of HONO. *Physical Chemistry Chemical Physics*, 8(17), 2028–2035. <https://doi.org/10.1039/b516590c>
- Belloli, R., Barletta, B., Bolzacchini, E., Meinardi, S., Orlandi, M., & Rindone, B. (1999). Determination of toxic nitrophenols in the atmosphere by high-performance liquid chromatography. *Journal of Chromatography A*, 846(1–2), 277–281. [https://doi.org/10.1016/S0021-9673\(99\)00030-8](https://doi.org/10.1016/S0021-9673(99)00030-8)
- Bianco, A., Passananti, M., Perroux, H., Voyard, G., Mouchel-Vallon, C., Chaumerliac, N., et al. (2015). A better understanding of hydroxyl radical photochemical sources in cloud waters collected at the puyde Dome station-experimental versus modelled formation rates. *Atmospheric Chemistry and Physics*, 15(16), 9191–9202. <https://doi.org/10.5194/acp-15-9191-2015>
- Birdsall, A. W., Andreoni, J. F., & Elrod, M. J. (2010). Investigation of the role of bicyclic peroxy radicals in the oxidation mechanism of toluene. *The Journal of Physical Chemistry A*, 114(39), 10,655–10,663. <https://doi.org/10.1021/jp105467e>
- Bohn, B., Corlett, G., Gillmann, M., Sanghavi, S., Stange, G., Tensing, E., et al. (2008). Photolysis frequency measurement techniques: Results of a comparison within the ACCENT project. *Atmospheric Chemistry and Physics*, 8, 5373–5391. <https://doi.org/10.5194/acp-8-5373-2008>
- Bolzacchini, E., Bruschi, M., Hjorth, J., Meinardi, S., Orlandi, M., Rindone, B., & Rosenbohm, E. (2001). Gas-phase reaction of phenol with NO<sub>3</sub>. *Environmental Science & Technology*, 35(9), 1791–1797. <https://doi.org/10.1021/es001290m>
- Bonnefoy, A., Chiron, S., & Botta, A. (2012). Environmental nitration processes enhance the mutagenic potency of aromatic compounds. *Environmental Toxicology*, 27(6), 321–331. <https://doi.org/10.1002/tox.20644>
- Cappa, C. D., Zhang, X., Loza, C. L., Craven, J. S., Lee, Y. D., & Seinfeld, J. H. (2013). Application of the statistical oxidation model (SOM) to secondary organic aerosol formation from photooxidation of C(12) alkanes. *Atmospheric Chemistry and Physics*, 13, 1591–1606. <https://doi.org/10.5194/acp-13-1591-2013>
- Chen, J., Wenger, J. C., & Venables, D. S. (2011). Near-ultraviolet absorption cross sections of nitrophenols and their potential influence on tropospheric oxidation capacity. *The Journal of Physical Chemistry A*, 115(44), 12,235–12,242. <https://doi.org/10.1021/jp206929r>
- Coggon, M. M., Veres, P. R., Yuan, B., Koss, A., Warneke, C., Gilman, J. B., et al. (2016). Emissions of nitrogen-containing organic compounds from the burning of herbaceous and arboraceous biomass: Fuel composition dependence and the variability of commonly used nitrile tracers. *Geophysical Research Letters*, 43, 9903–9912. <https://doi.org/10.1002/2016GL070562>
- Dang, C., Bannan, T., Shelley, P., Priestley, M., Worrall, S. D., Waters, J., et al. (2019). The effect of structure and isomerism on the vapor pressures of organic molecules and its potential atmospheric relevance. *Aerosol Science and Technology*, 53(9), 1040–1055. <https://doi.org/10.1080/02786826.2019.1628177>
- De Gouw, J. A., Warneke, C., Parrish, D. D., Holloway, J. S., Trainer, M., & Fehsenfeld, F. C. (2003). Emission sources and ocean uptake of acetonitrile (CH<sub>3</sub>CN) in the atmosphere. *Journal of Geophysical Research*, 108(D11), 4329–4336. <https://doi.org/10.1029/2002JD002897>
- Desyaterik, Y., Sun, Y., Shen, X., Lee, T., Wang, X., Wang, T., & Collett, J. L. (2013). Speciation of “brown” carbon in cloud water impacted by agricultural biomass burning in eastern China. *Journal of Geophysical Research: Atmospheres*, 118, 7389–7399. <https://doi.org/10.1002/jgrd.50561>
- Evans, M. J., & Jacob, D. J. (2005). Impact of new laboratory studies of N<sub>2</sub>O<sub>5</sub> hydrolysis on global model budgets of tropospheric nitrogen oxides, ozone, and OH. *Geophysical Research Letters*, 32, L09813. <https://doi.org/10.1029/2005GL022469>
- Gilman, J., Lerner, B., Kuster, W., Goldan, P., Warneke, C., Veres, P., et al. (2015). Biomass burning emissions and potential air quality impacts of volatile organic compounds and other trace gases from fuels common in the US. *Atmospheric Chemistry and Physics*, 15, 13,915–13,938. <https://doi.org/10.5194/acp-15-13915-2015>
- Grosjean, D. (1984). Atmospheric reactions of ortho cresol: Gas phase and aerosol products. *Atmospheric Environment*, 18(8), 1641–1652. [https://doi.org/10.1016/0004-6981\(84\)90386-X](https://doi.org/10.1016/0004-6981(84)90386-X)
- Harrison, M., Heal, M., & Cape, J. (2005). Evaluation of the pathways of tropospheric nitrophenol formation from benzene and phenol using a multiphase model. *Atmospheric Chemistry and Physics*, 5, 1679–1695. <https://doi.org/10.5194/acp-5-1679-2005>
- Harrison, M. A., Barra, S., Borghesi, D., Vione, D., Arsene, C., & Olariu, R. I. (2005). Nitrated phenols in the atmosphere: A review. *Atmospheric Environment*, 39(2), 231–248. <https://doi.org/10.1016/j.atmosenv.2004.09.044>
- Hu, W. W., Hu, M., Deng, Z. Q., Xiao, R., Kondo, Y., Takegawa, N., et al. (2012). The characteristics and origins of carbonaceous aerosol at a rural site of PRD in summer of 2006. *Atmospheric Chemistry and Physics*, 12(4), 1811–1822. <https://doi.org/10.5194/acp-12-1811-2012>
- Huang, D. D., Zhang, X., Dalleska, N. F., Lignell, H., Coggon, M. M., Chan, C. M., et al. (2016). A note on the effects of inorganic seed aerosol on the oxidation state of secondary organic aerosol—A-pinene ozonolysis. *Journal of Geophysical Research: Atmospheres*, 121, 12–476. <https://doi.org/10.1002/2016JD025999>
- Huang, Y., Zhao, R., Charan, S. M., Kenseth, C. M., Zhang, X., & Seinfeld, J. H. (2018). Unified theory of vapor-wall mass transport in teflon-walled environmental chambers. *Environmental Science & Technology*, 52(4), 2134–2142. <https://doi.org/10.1021/acs.est.7b05575>
- Iinuma, Y., Böge, O., Gräfe, R., & Herrmann, H. (2010). Methyl-nitrocatechols: Atmospheric tracer compounds for biomass burning secondary organic aerosols. *Environmental Science & Technology*, 44(22), 8453–8459. <https://doi.org/10.1021/es102938a>
- Inomata, S., Tanimoto, H., Pan, X., Taketani, F., Komazaki, Y., Miyakawa, T., et al. (2015). Laboratory measurements of emission factors of nonmethane volatile organic compounds from burning of Chinese crop residues. *Journal of Geophysical Research: Atmospheres*, 120, 5237–5252. <https://doi.org/10.1002/2014jd022761>
- Jacobson, M. Z. (1999). Isolating nitrated and aromatic aerosols and nitrated aromatic gases as sources of ultraviolet light absorption. *Journal of Geophysical Research*, 104(D3), 3527–3542. <https://doi.org/10.1029/1998JD100054>

- Ji, Y., Zhao, J., Terazono, H., Misawa, K., Levitt, N. P., Li, Y., et al. (2017). Reassessing the atmospheric oxidation mechanism of toluene. *Proceedings of the National Academy of Sciences USA*, *114*(31), 8169–8174. <https://doi.org/10.1073/pnas.1705463114>
- Jing, B., Tong, S., Liu, Q., Li, K., Wang, W., Zhang, Y., & Ge, M. (2016). Hygroscopic behavior of multicomponent organic aerosols and their internal mixtures with ammonium sulfate. *Atmospheric Chemistry and Physics*, *16*(6), 4101–4118. <https://doi.org/10.5194/acp-16-4101-2016>
- Jobson, B. T., Volkamer, R. A., Velasco, E., Allwine, G., Westberg, H., Lamb, B. K., et al. (2011). Comparison of aromatic hydrocarbon measurements made by PTR-MS, DOAS and GC-FID during the MCMA 2003 field experiment. *Atmospheric Chemistry and Physics*, *10*, 1989–2005. <https://doi.org/10.5194/acp-10-1989-2010>
- Kitanovski, Z., Grgić, I., Vermeylen, R., Claeys, M., & Maenhaut, W. (2012). Liquid chromatography tandem mass spectrometry method for characterization of monoaromatic nitro-compounds in atmospheric particulate matter. *Journal of Chromatography A*, *1268*, 35–43. <https://doi.org/10.1016/j.chroma.2012.10.021>
- Klotz, B., Sørensen, S., Barnes, I., Becker, K. H., Eitzkorn, T., Volkamer, R., et al. (1998). Atmospheric oxidation of toluene in a large-volume outdoor photoreactor: In situ determination of ring-retaining product yields. *The Journal of Physical Chemistry A*, *102*(50), 10,289–10,299. <https://doi.org/10.1021/jp982719n>
- Krechmer, J. E., Coggon, M. M., Massoli, P., Nguyen, T. B., Crounse, J. D., Hu, W., et al. (2015). Formation of low volatility organic compounds and secondary organic aerosol from isoprene hydroxyhydroperoxide low-NO oxidation. *Environmental Science & Technology*, *49*(17), 10,330–10,339. <https://doi.org/10.1021/acs.est.5b02031>
- Kudo, S., Tanimoto, H., Inomata, S., Saito, S., Pan, X., Kanaya, Y., et al. (2014). Emissions of nonmethane volatile organic compounds from open crop residue burning in the Yangtze River Delta region, China. *Journal of Geophysical Research: Atmospheres*, *119*, 7684–7698. <https://doi.org/10.1002/2013JD021044>
- Laskin, A., Laskin, J., & Nizkorodov, S. A. (2015). Chemistry of atmospheric brown carbon. *Chemical Reviews*, *115*(10), 4335–4382. <https://doi.org/10.1021/cr5006167>
- Leuenberger, C., Czuczwa, J., Tremp, J., & Giger, W. (1988). Nitrated phenols in rain: Atmospheric occurrence of phytotoxic pollutants. *Chemosphere*, *17*(3), 511–515. [https://doi.org/10.1016/0045-6535\(88\)90026-4](https://doi.org/10.1016/0045-6535(88)90026-4)
- Levsen, K., Behnert, S., Musmann, P., Raabe, M., & Priess, B. (1993). Organic compounds in cloud and rain water. *International Journal of Environmental Analytical Chemistry*, *52*(1–4), 87–97. <https://doi.org/10.1080/03067319308042851>
- Liu, X. L., Zeng, L. M., Lu, S. H., & Yu, X. N. (2009). Online monitoring system for volatile organic compounds in the atmosphere. *Acta Scientiae Circumstantiae*, *29*(12), 2471–2477.
- Lüttke, J., Levsen, K., Acker, K., Wieprecht, W., & Möller, D. (1999). Phenols and nitrated phenols in clouds at Mount Brocken. *International Journal of Environmental Analytical Chemistry*, *74*(1–4), 69–89. <https://doi.org/10.1080/03067319908031417>
- McVay, R. C., Zhang, X., Aumont, B., Valorso, R., Camredon, M., La, Y. S., et al. (2016). SOA formation from the photooxidation of  $\alpha$ -pinene: Systematic exploration of the simulation of chamber data. *Atmospheric Chemistry and Physics*, *16*(5), 2785–2802. <https://doi.org/10.5194/acp-16-2785-2016>
- Nah, T., McVay, R. C., Zhang, X., Boyd, C. M., Seinfeld, J. H., & Ng, N. L. (2016). Influence of seed aerosol surface area and oxidation rate on vapor wall deposition and SOA mass yields: A case study with  $\alpha$ -pinene ozonolysis. *Atmospheric Chemistry and Physics*, *16*(14), 9361–9379. <https://doi.org/10.5194/acp-16-9361-2016>
- Olariu, R., Barnes, I., Bejan, I., Arsene, C., Vione, D., Klotz, B., & Becker, K. (2013). FT-IR product study of the reactions of NO<sub>3</sub> radicals with ortho-, meta-, and para-cresol. *Environmental Science & Technology*, *47*(14), 7729–7738. <https://doi.org/10.1021/es401096w>
- Olariu, R. I., Klotz, B., Barnes, I., Becker, K. H., & Mocanu, R. (2002). FT-IR study of the ring-retaining products from the reaction of OH radicals with phenol, o-, m-, and p-cresol. *Atmospheric Environment*, *36*(22), 3685–3697. [https://doi.org/10.1016/S1352-2310\(02\)00202-9](https://doi.org/10.1016/S1352-2310(02)00202-9)
- Paulson, S. E., Gallimore, P. J., Kuang, X. M., Chen, J. R., Kalberer, M., & Gonzalez, D. H. (2019). A light-driven burst of hydroxyl radicals dominates oxidation chemistry in newly activated cloud droplets. *Science Advances*, *5*(5), eaav7689. <https://doi.org/10.1126/sciadv.aav7689>
- Rippen, G., Zietz, E., Frank, R., Knacker, T., & Klöpffer, W. (1987). Do airborne nitrophenols contribute to forest decline? *Environmental Science & Technology*, *8*, 475–482. <https://doi.org/10.1080/09593338709384508>
- Sander, R. (2015). Compilation of Henry's law constants (version 4.0) for water as solvent. *Atmospheric Chemistry and Physics*, *15*, 4399–4981. <https://doi.org/10.5194/acp-15-4399-2015>
- Sangwan, M., & Zhu, L. (2016). Absorption cross sections of 2-nitrophenol in the 295–400 nm region and photolysis of 2-nitrophenol at 308 and 351 nm. *The Journal of Physical Chemistry A*, *120*(50), 9958–9967. <https://doi.org/10.1021/acs.jpca.6b08961>
- Scala, A. J., & Banerjee, S. (1982). *Vapor pressure laboratory report*. Syracuse, NY: Syracuse Research Corporation.
- Schwantes, R. H., McVay, R. C., Zhang, X., Coggon, M. M., Lignell, H., Flagan, R. C., et al. (2017). Science of the environmental chamber. In *Advances in atmospheric chemistry*. NJ: World Scientific.
- Schwantes, R. H., Schilling, K. A., McVay, R. C., Lignell, H., Coggon, M. M., Zhang, X., et al. (2017). Formation of highly oxygenated low-volatility products from cresol oxidation. *Atmospheric Chemistry and Physics*, *17*, 3453–3474. <https://doi.org/10.5194/acp-17-3453-2017>
- Seinfeld, J. H., & Pandis, S. N. (2016). *Atmospheric chemistry and physics: From air pollution to climate change*. Hoboken, NJ: John Wiley & Sons.
- Smith, D., McIver, C., & Kleindienst, T. (1998). Primary product distribution from the reaction of hydroxyl radicals with toluene at ppb NO<sub>x</sub> mixing ratios. *Journal of Atmospheric Chemistry*, *30*(2), 209–228. <https://doi.org/10.1023/A:1005980301720>
- Stockwell, C., Veres, P., & Williams, J. (2015). Characterization of biomass burning emissions from cooking fires, peat, crop residue, and other fuels with high-resolution proton-transfer-reaction time-of-flight mass spectrometry. *Atmospheric Chemistry and Physics*, *15*, 845–865. <https://doi.org/10.5194/acp-15-845-2015>
- Vione, D., Maurino, V., Minero, C., Duncianu, M., Olariu, R.-I., Arsene, C., et al. (2009). Assessing the transformation kinetics of 2- and 4-nitrophenol in the atmospheric aqueous phase. Implications for the distribution of both nitroisomers in the atmosphere. *Atmospheric Environment*, *43*(14), 2321–2327. <https://doi.org/10.1016/j.atmosenv.2009.01.025>
- Vione, D., Maurino, V., Minero, C., & Pelizzetti, E. (2001). Phenol photolysis upon UV irradiation of nitrite in aqueous solution I: Effects of oxygen and 2-propanol. *Chemosphere*, *45*(6–7), 893–902. [https://doi.org/10.1016/s0045-6535\(01\)00035-2](https://doi.org/10.1016/s0045-6535(01)00035-2)
- Wang, H. L., Huang, D., Zhang, X., Zhao, Y., & Chen, Z. M. (2012). Understanding the aqueous phase ozonolysis of isoprene: Distinct product distribution and mechanism from the gas phase reaction. *Atmospheric Chemistry and Physics*, *12*(15), 7187–7198. <https://doi.org/10.5194/acp-12-7187-2012>

- Wang, S., McNamara, S. M., Moore, C. W., Obrist, D., Steffen, A., Shepson, P. B., et al. (2019). Direct detection of atmospheric atomic bromine leading to mercury and ozone depletion. *Proceedings of the National Academy of Sciences USA*, *116*(29), 14,479–14,484. <https://doi.org/10.1073/pnas.1900613116>
- Wennberg, P. O., Bates, K. H., Crounse, J. D., Dodson, L. G., McVay, R. C., Mertens, L. A., et al. (2018). Gas-phase reactions of isoprene and its major oxidation products. *Chemical Reviews*, *118*(7), 3337–3390. <https://doi.org/10.1021/acs.chemrev.7b00439>
- Yuan, B., Liggio, J., Wentzell, J., Li, S.-M., Stark, H., Roberts, J. M., et al. (2016). Secondary formation of nitrated phenols: Insights from observations during the Uintah Basin Winter Ozone Study (UBWOS) 2014. *Atmospheric Chemistry and Physics*, *16*(4), 2139–2153. <https://doi.org/10.5194/acp-16-2139-2016>
- Zhang, X., Cappa, C. D., Jathar, S. H., McVay, R. C., Ensberg, J. J., Kleeman, M. J., & Seinfeld, J. H. (2014). Influence of vapor wall loss in laboratory chambers on yields of secondary organic aerosol. *Proceedings of the National Academy of Sciences*, *111*(16), 5802–5807. <https://doi.org/10.1073/pnas.1404727111>
- Zhang, X., Chen, Z., Wang, H., He, S., & Huang, D. (2009). An important pathway for ozonolysis of alpha-pinene and beta-pinene in aqueous phase and its atmospheric implications. *Atmospheric Environment*, *43*(29), 4465–4471. <https://doi.org/10.1016/j.atmosenv.2009.06.028>
- Zhang, X., Ortega, J., Huang, Y., Shertz, S., Tyndall, G. S., & Orlando, J. J. (2018). A steady-state continuous flow chamber for the study of daytime and nighttime chemistry under atmospherically relevant NO levels. *Atmospheric Measurement Techniques*, *11*(5), 2537–2551. <https://doi.org/10.5194/amt-11-2537-2018>
- Zhang, X., Schwantes, R., McVay, R., Lignell, H., Coggon, M., Flagan, R., & Seinfeld, J. (2015). Vapor wall deposition in Teflon chambers. *Atmospheric Chemistry and Physics*, *15*(8), 4197–4214. <https://doi.org/10.5194/acp-15-4197-2015>
- Zhang, X., & Seinfeld, J. H. (2013). A functional group oxidation model (FGOM) for SOA formation and aging. *Atmospheric Chemistry and Physics*, *13*(12), 5907–5926. <https://doi.org/10.5194/acp-13-5907-2013>